Journal of Physics:
Condensed Matter

PAPER

Large enhancement of effective spin–orbit torque efficiency by optimizing the capping layer thickness in Ta/Pt/Co trilayer

To cite this article: Zhan Xu *et al* 2025 *J. Phys.: Condens. Matter* **37** 475801

IOP Publishing Journal of Physics: Condensed Matter
J. Phys.: Condens. Matter **37** (2025) 475801 (8pp) https://doi.org/10.1088/1361-648X/ae1d04

Large enhancement of effective spin–orbit torque efficiency by optimizing the capping layer thickness in Ta/Pt/Co trilayer

Zhan Xu[1,2,*], Shuo Wu[2], Runtian Li[3], Wenwen Liu[3], Er Liu[3], Leixiang Bian[1], Feng Xu[3], Jiaxuan Tang[4,*] and Wen Siang Lew[2,*]

[1] School of Safety Science and Engineering, Nanjing University of Science and Technology, Nanjing 210094, People's Republic of China
[2] School of Physical and Mathematical Sciences, Nanyang Technological University, 21 Nanyang Link, Singapore 637371, Singapore
[3] MIIT Key Laboratory of Advanced Metallic and Intermetallic Materials Technology, School of Materials Science and Engineering, Nanjing University of Science and Technology, Nanjing 210094, People's Republic of China
[4] School of Materials Engineering, Jinling Institute of Technology, Nanjing 210038, People's Republic of China

E-mail: zhanxu@njust.edu.cn, tangjx@jit.edu.cn and wensiang@ntu.edu.sg

Received 1 October 2025, revised 28 October 2025
Accepted for publication 7 November 2025
Published 18 November 2025

Abstract

We report the influence of the capping layer thickness on the effective magnetic damping and the effective spin–orbit torque (SOT) efficiency in Ta/Pt/Co structures via spin-torque ferromagnetic resonance measurements. The SOT efficiency first increases with increasing capping layer thickness (d_{Ta}), *reaching a large value of 0.199 at* $d_{Ta} = 1.4$ nm, then decreases with further increases in d_{Ta}. This can be attributed to a competition between the additional SOT field generated by the Rashba–Edelstein effect and the reduced net spin current effect. It has been demonstrated that the magnetic damping factor decreases with increasing capping layer thickness. The high SOT efficiency and low magnetic damping factor suggest the great potential of the Ta/Pt/Co for low-power spintronic technologies.

Supplementary material for this article is available online

Keywords: SOT efficiency, magnetic damping factor, interfacial effect, ST-FMR

1. Introduction

Spin–orbit torques (SOTs) have attracted significant attention as an effective means to electrically regulate the magnetization direction of magnetic materials [1–4]. The next generation of spintronics devices based on SOT has been widely used in SOT magnetic random-access memory (SOT-MRAM), spin-nano-oscillator, and magnetic logic devices due to their significant advantages of high-speed operation and ultra-low energy consumption [2]. The generation mechanism of SOT encompasses multiple physical pathways, including the spin Hall effect (SHE), the Rashba–Edelstein effect (REE), the orbital Hall effect, and magnons [1]. Specifically, SHE occurs primarily within the bulk material, relying on spin–orbit coupling to generate a transverse spin current, with the strength

* Authors to whom any correspondence should be addressed.

of this effect depending significantly on the strength of spin–orbit coupling within the material. In contrast, REE arises from structural inversion symmetry breaking, leading to spin accumulation at the interface, which is related to the spin–orbit coupling at the interface and the interface scattering situation.

Enhancing SOT efficiency ξ_{SOT} (defined as the ratio of the spin current density J_s to the charge current density J_c) is pivotal in reducing the device's power consumption [3]. Consequently, developing new materials and exploring novel physical mechanisms to enhance the performance of SOT devices have emerged as key objectives in current research. To date, researchers have conducted in-depth studies on heavy metals (HMs) and their alloys [5–7], antiferromagnetic materials [8], oxides [9], and transition metal dichalcogenides [10].

Recently, there has been a surge of interest in the effects of different HM/FM and HM-alloy/FM interface combinations on SOT efficiency [11–15]. A variety of interface-engineering techniques have been employed to facilitate SOT enhancement. It has been demonstrated that incorporating two heavy-metal layers with opposite SOT efficiency signs on opposing sides of the ferromagnetic layer can enhance the SOT efficiency in the multilayer [16]. It has long been hypothesized that the net spin-moment generation efficiency in the HM1/HM2/FM system is diminished when two layers of HMs with opposite spin Hall angles are used, such as W and Pt, or Ta and Pt. However, Ma *et al* demonstrated that a heavy-metal bilayer structure with opposite spin Hall angles can facilitate competing spin current generation in Pt/W/CoFeB [17]. The out-of-plane effective field can achieve field-free SOT switching of a perpendicular CoFeB layer. An enhanced spin Hall magnetoresistance due to spin accumulation has been observed in Pt/$Y_3Fe_5O_{12}$ (YIG) with a capping layer [18]. Similarly, Hui *et al* also reported that the net spin current at the Pt/NiFe interface was modulated by tailoring the thickness of the Ta capping layer, which enhanced the spin accumulation at the Pt/NiFe interface [19]. Karube *et al* demonstrated the additional SOT field generation at the W/Pt interface under the REE [20]. Very recently, Li *et al* have reported a large orbital–spin conversion in the Ta/Pt/$Tm_3Fe_5O_{12}$ heterostructure due to the conversion of the orbital currents generated by Ta into spin currents in the Pt interior by the orbital Hall effect [21]. However, achieving both a low effective damping factor and high SOT efficiency is crucial for driving the adoption of SOT devices, as it helps to minimize the critical switching current [22]. Among existing techniques, spin-torque ferromagnetic resonance (ST-FMR) is a popular and powerful tool for quantifying SOT, as it can simultaneously characterize SOT efficiency and the damping magnetic factor [23].

In this work, we investigate the influence of the capping layer thickness on the effective magnetic damping and SOT efficiency in the Ta/Pt/Co trilayer via the ST-FMR measurements technique. The findings indicate that the Ta capping layer reduces effective magnetic damping by 35% while concurrently increasing SOT efficiency by 1.3-fold relative to that observed in Co/Pt. As the Ta layer thickness increases, the effective SOT efficiency initially rises, attains a maximum at $d_{Ta} = 1.4$ nm, and subsequently declines as the thickness increases further. This might be attributed to the additional SOT field contribution engendered by the interfacial REE, which arises from the spin accumulation at the Ta/Pt interface. Meanwhile, the effective damping factor declines rapidly with increasing Ta layer thickness. For thicknesses greater than 1.2 nm, the effective damping factor shows a tendency toward stability. Moreover, the calculated minimum critical switching current density can be reduced by 46%.

2. Experiment

The film stacks were deposited by direct current (DC) sputtering onto thermally oxidized silicon substrates at an argon (Ar) partial pressure of 0.27 Pa. The base pressure of the sputter chamber was maintained below 1.33×10^{-8} Pa. The film stacks were composed of the following layers: Ta(d_{Ta})/Pt(5 nm)/Co(5 nm)/Si(SiO_2), with d_{Ta} ranging from 0 to 5 nm. The thickness of the stack was calibrated using an atomic force microscope [24]. The crystal quality and magnetic properties were examined using x-ray diffraction (XRD) and a vibrating sample magnetometer (VSM). For ST-FMR measurements, the Ta/Pt/Co stacks were patterned into rectangular-shaped strips with a width of 10 μm and a length of 50 μm. This was achieved using electron beam lithography and argon ion milling, respectively. Ta (5 nm)/Cu (200 nm)/Pt (3 nm) electrodes were subsequently deposited on the patterned structures using a combination of electron-beam lithography and lift-off. An illustration of the measurement setup and device, and a detailed optical image of the patterned structure, is provided in figure 1(a).

In an ST-FMR measurement, a microwave radio frequency (RF) charge current traverses the SOT material, giving rise to an AC SOT, which induces FMR of the adjacent FM [5, 25]. The oscillating SOT will cause oscillations in the resistance, attributed to the anisotropic magnetoresistance of the FM layer. Mixing the RF current with the oscillating resistance using a bias tee yields a rectified DC voltage signal (V_{mix}). To ensure that the measured DC voltage is within the linear range and that the microwave heating effect is negligible, the input microwave power is set to 18 dBm (see supplement material). All measurements were performed at room temperature. The detailed methodology for the ST-FMR measurements is described in earlier reports [5, 22].

3. Results and discussion

The XRD pattern for the Pt(5 nm)/Co(5 nm) film in the range of 35°–50° is shown in figure 1(b). Two strong diffraction peaks corresponding to Pt(111) and Co(002) are observed at 39.8° and 44.7°, respectively, indicating that the bilayer has a well-ordered crystal structure. Figure 1(c) illustrates the *M*–*H* loops of the Ta(1.4 nm)/Pt(5 nm)/Co(5 nm) film in both in-plane and out-of-plane directions, which demonstrate in-plane magnetic anisotropy. The saturation magnetization

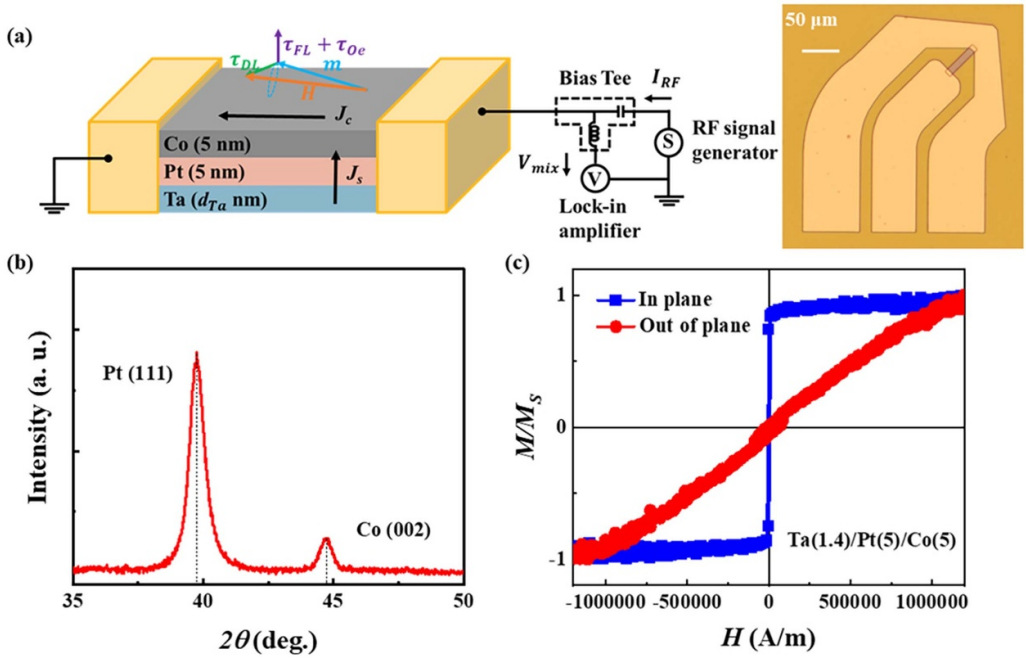

Figure 1. (a) Schematic illustration of the Ta/Pt/Co multilayer device for the ST-FMR measurement. The $\tau_{FL}+\tau_{Oe}$ term denotes the sum of the field-like torque and the Oersted field torque, while τ_{DL} is the damping-like torque. J_c and J_s are the charge current density and the spin current density, respectively. The inset is the optical image of the fabricated device and electrodes. (b) XRD patterns for Pt(5 nm)/Co(5 nm) film grown on Si(100) substrates. (c) *M*–*H* loops for Ta(1.4 nm)/Pt(5 nm)/Co(5 nm) film.

measured by VSM is 1067 kA m^{-1}, consistent with previous reports [12].

Figure 2(a) shows the ST-FMR spectra for the Ta(1.4 nm)/Pt(5 nm)/Co(5 nm) sample measured with an external in-plane magnetic field applied at an angle of 45 degrees with respect to the longitudinal direction of the device. The ST-FMR spectra were measured over a microwave frequency range of 10–22 GHz. As the frequency increases, the resonance field H_{res} increases accordingly. Figure 2(b) shows the example of ST-FMR spectra for Ta(d_{Ta})/Pt(5 nm)/Co(5 nm) at a fixed frequency of 14 GHz. The FMR curves show a downward shift in the resonance field with increasing Ta thickness. This resonance field shift for $d_{Ta} > 0.6$ nm indicates an increase in the effective magnetization of the Co layer [26]. Figures 2(b) and (c) show a detailed and representative fit result of the ST-FMR spectrum at $f = 14$ GHz for $d_{Ta} = 0$ nm and 1.4 nm, respectively. The ST-FMR spectra can be fitted by $V_{mix} = S \cdot F_S + A \cdot F_A + C$, where F_S and F_A are the symmetric $\left\{\Delta^2/\left[(H-H_{res})^2+\Delta^2\right]\right\}$ and asymmetric Lorentzian function components $\left\{\Delta(H-H_{res})/\left[(H-H_{res})^2+\Delta^2\right]\right\}$, S and A are the amplitudes of the symmetric and antisymmetric components of the mixing voltage, Δ is the resonance linewidth, H_{res} is the resonance magnetic field, and C is a constant representing the voltage offset [25]. In the ST-FMR signal, the symmetric component is proportional to the damping-like effective torque. In contrast, the anti-symmetric component results from the summation of the Oersted field torque and the field-like effective torque. The Oersted field of microwave is considered to be the only contribution to field-like torque, while damping-like torque is mainly caused by spin current converted from charge current flowing in the HM layer, which can be attributed to SHE and/or the REE [25]. According to previous work, the spin-pumping voltage signal has a negligible impact on the symmetric voltage component [10, 22].

The symmetric (V_S) and antisymmetric (V_A) contributions of the Lorentzian line shapes are represented by the red and blue curves, as shown in figures 2(c) and (d), respectively. It can be observed that the V_{mix} at $d_{Ta} = 1.4$ nm is slightly smaller than that at $d_{Ta} = 0$ nm, which may be attributed to the shunt effect. Furthermore, it can be observed that there is minimal distinction between the symmetric and asymmetric components.

Moreover, we examine the variation in SOT efficiency with Ta layer thickness. The effective SOT efficiency is estimated as the ratio of the spin current density to the RF current density. It can be calculated from the line shape of ST-FMR spectra. It is given by [25],

$$\xi_{SOT} = \frac{J_S}{J_C} = \frac{S}{A}\frac{e\mu_0 M_S t_{Co} d_{HM}}{\hbar}\left(1+\frac{M_{eff}}{H_{res}}\right)^{1/2} \quad (1)$$

where J_S is the spin current density generated within the HM, J_C is the applied charge current density, and t_{Co} and d_{HM} are the thicknesses of Co and HM layers, respectively. In equation (1), we use the Pt layer thickness as the heavy-metal layer thickness. The effective SOT efficiency as a function of

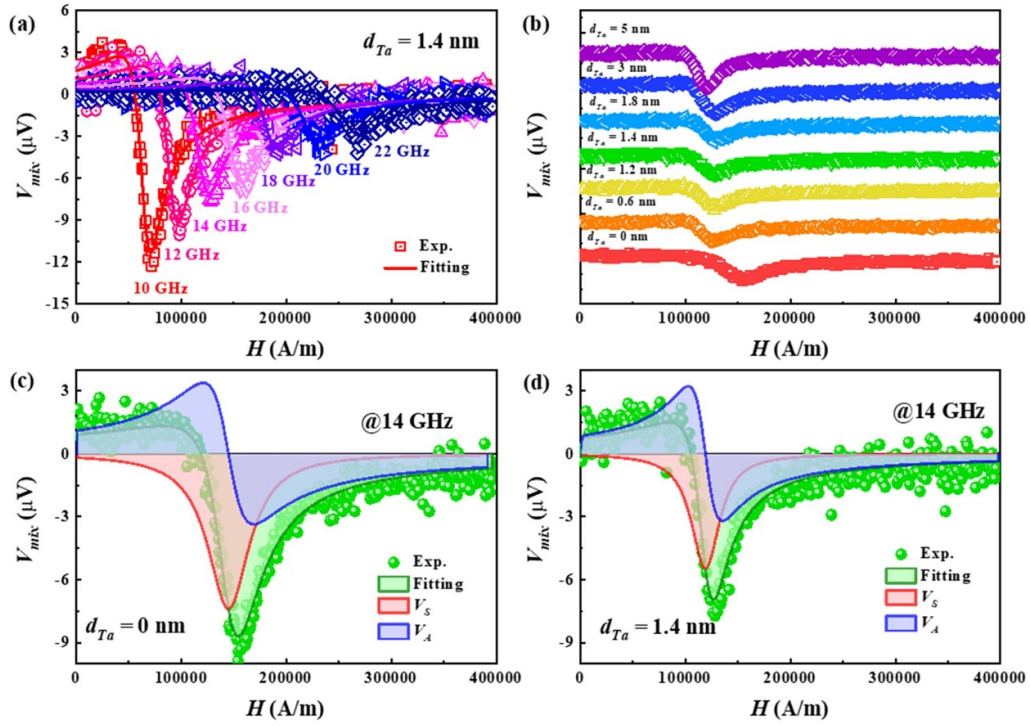

Figure 2. (a) The ST-FMR spectra of Ta(1.4 nm)/Pt(5 nm)/Co(5 nm) film from 10 to 22 GHz with fitted curves. (b) The ST-FMR spectra at a fixed frequency of 14 GHz for Ta/Pt/Co samples with varying d_{Ta}. V_{mix}, along with the fitted (green), symmetric (V_{S}, red), and asymmetric (V_{A}, blue) Lorentzian functions used for the fitting, measured at 14 GHz for Ta capping layer thicknesses of 0 nm (c) and 1.4 nm (d).

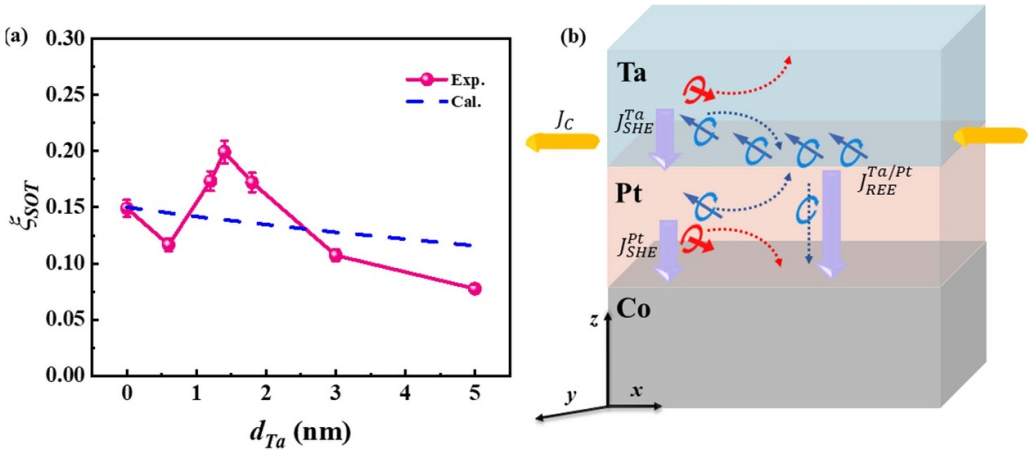

Figure 3. (a) The effective SOT efficiency as a function of Ta capping layer thickness. The dashed lines are calculated curves based on a parallel circuit model. (b) A schematic illustration of the generation and transport of the spin current and orbital current in the Ta/Pt/Co heterostructure.

Ta thickness is plotted in figure 3(a). The ξ_{SOT} changes non-monotonically with increasing d_{Ta}. A rapid increase in ξ_{SOT} is observed when the thickness of the Ta layer is less than 1.4 nm, reaching a maximum value as large as 0.199 at 1.4 nm, after which it exhibits a gradual decline as the thickness increases. It was determined that the ξ_{SOT} of the Ta(5)/Pt(5)/Co(5) sample reduced to 0.077. A large increase (33.6%) in the effective SOT efficiency for $d_{\mathrm{Ta}} = 1.4$ nm was observed compared to $d_{\mathrm{Ta}} = 0$ nm. This demonstrates that, while the charge-spin conversion efficiency resulting from the REE at the Ta/Pt interface is lower than the contribution from the bulk SHE, it is still considerable. It is to be noted that the SOT efficiency of all Ta/Pt multilayer films is positive, as indicated by the sign of the *S*/*A*. This suggests that adding the Ta layer does not change the sign of the spin Hall angle, likely because Ta's spin Hall angle is relatively small compared to Pt's. Meanwhile, the SOT efficiency of the pure Ta layer was found to be −0.03 (see supplement material).

Applying the parallel circuit model with the resistivity of Ta, Co, and Pt (199, 30, and 47 $\mu\Omega$ cm) [16, 27], yielded a

current percentage range of 39.0%–35.7% through the Pt layer and 0%–8.4% went through the Ta layer, in the thickness of the Ta capping layer from 0 to 5 nm. It is noted that the current through the Ta layer increases monotonically. In contrast, the current through the Pt layer decreases monotonically as the Ta layer thickness increases. Given the opposite SHA signs of Pt (0.15) and Ta (−0.03), the overall SOT efficiency is expected to decrease monotonically if no additional interfacial contributions are present, as shown in figure 3(a). As the spin currents with opposite polarization directions cancel each other out, the SOT efficiency of the HM bilayer structure is lower than that of the single-layer HM structure in the absence of additional SOT effects, which is different from the variation of the effective SOT efficiency with respect to the Ta capping layer thickness shown in figure 3(a). And similar SOT enhancement is observed in both Pt/W/Py and W/Pt/Py film stacks, which is caused by the non-equilibrium spin accumulation at the W/Pt interface via REE. As shown in figure 3(b), spin currents are generated in the Ta layer by applying a charge current along the *x*-direction due to the SHE which is used to reach the Ta/Pt interface. However, the Pt thicknesses employed in our system are all in the range of 5 nm, which is larger than the spin diffusion length of Pt in the Pt/Co system (2.1 nm, see supplement material). Therefore, the spin current in the Ta layer, due to the bulk contribution of the SHE is impeded from crossing the Pt layer, resulting in a greater accumulation of spin current at the Ta/Pt interface. The Ta and Pt layers exhibit opposite spin Hall angles, resulting in spin currents with opposite polarizations. The generation of the additional SOT field primarily arises from the following four processes: (1) accumulation of REE spins at the Ta/Pt interface, (2) conversion of spin current at the Ta/Pt interface into orbital current, (3) diffusion transport of orbital current within Pt, and (4) conversion of orbital current into spin current due to strong spin coupling in the Pt layer, which is subsequently absorbed by the Co layer.

Thus, the nonmonotonic variation of SOT efficiency might be ascribed to a competition between the additional SOT field, which is generated by the interfacial REE originating from spin accumulation, and the reduced net spin current effect. Based on the Luan *et al* model [18], owing to the opposite spin Hall angles of Pt and Ta, the spin-dependent chemical potentials of Pt and Ta have the same sign at the Ta/Pt interface. At small thicknesses, the Ta layer primarily serves as a spin sink, enhancing spin accumulation at the Ta/Pt interface and thereby generating an additional SOT field. On the other hand, as the Ta layer thickness increases, the shunting effect intensifies, allowing more charge current to flow into the Ta layer. At the same time, as the spins generated by the REE at the Ta/Pt interface diffuse into the Ta layer, the net spin current at the interface decreases as the Ta layer becomes thicker [20]. In the case of a thin Ta layer, the additional SOT field has a dominant influence, leading to enhanced SOT efficiency. Conversely, in the presence of a thicker Ta layer, the opposing sign of the spin Hall angles results in a net spin current reduction effect that outweighs the influence of the additional SOT field, resulting in a continuous decrease in SOT efficiency. This is consistent with the damping-like torque enhancement observed in W/Pt/CoFeB multilayers [28]. In their work, even though the Pt thickness is 5 nm, the additional 3 nm thick W layer still enhances SOT efficiency.

The effective magnetization (M_{eff}) values were determined by fitting the resonance frequency (f) as a dependence on the resonance field (H_{res}) in figure 4(a) using the Kittel formula, given the negligible in-plane magnetic anisotropy. The Kittel equation can be written as $f = \gamma[H_{\mathrm{res}}\,(H_{\mathrm{res}} + M_{\mathrm{eff}})]^{1/2}$, where γ is the gyromagnetic ratio [29]. The obtained M_{eff} as a function of d_{Ta} is shown in figure 4(b). When the Ta thickness is 0, the M_{eff} is 1.3 T, consistent with previously reported results [22]. As the Ta thickness increases, the effective magnetization rises, and M_{eff} remains approximately 1.55 T even after d_{Ta} exceeds 1.2 nm.

To determine the effective damping constant α_{eff}, the frequency-dependent linewidths for different Ta thicknesses are plotted in figure 4(c). It demonstrates that there is no deviation from a strict linear correlation across the entire frequency spectrum, indicating that the two-magnon scattering mechanisms in the film have a minimal impact and do not result in a nonlinear trend. Furthermore, the $d_{\mathrm{Ta}} = 0$ nm slope is considerably steeper than at other thicknesses. This indicates that incorporating the Ta layer reduces the system's damping factor.

To examine the variation of the damping factor concerning d_{Ta}, the variation of the damping factor concerning the Ta thickness is obtained through linear fitting via the equation $\Delta H = \Delta H_{\mathrm{inh}} + f\alpha_{\mathrm{eff}}/\gamma$ [30], as illustrated in figure 4(d). Here, the inhomogeneous linewidth ΔH_{inh} results from the inhomogeneity of the magnetic films and depends on the lattice mismatch at the HM/FM interface [31]. From the fitting, the value of α_{eff} for $d_{\mathrm{Ta}} = 0$ nm is 0.0260, consistent with the previously reported value of Pt/Co. It is indicated that disparate trends are observed between the magnetic damping factor and the SOT efficiency, suggesting that alternative mechanisms may underlie the observed shifts in these variables.

As the Ta thickness increases from 0 to 1.2 nm, the magnetic damping factor decreases rapidly to ∼0.014, and as the thickness continues to rise, the damping factor remains at 0.017–0.014. The relationship between α_{eff} and the Ta capping layer thickness is found to closely follow an exponential phenomenological expression: $\alpha_{\mathrm{eff}} \propto a\mathrm{e}^{-d_{\mathrm{Ta}}/b} + c$ in which the parameters $a = 0.011$, $b = 0.58$ nm, and $c = 0.015$ [20]. In the exponential phenomenological expression, a represents the variable magnetic damping factor, b is a length parameter associated with the spin diffusion coefficient, and c denotes a constant representing the damping offset. It can be observed that the magnetic damping factor values remain larger than the intrinsic magnetic damping factor values of Co monolayer films. The reduction of the Co magnetic damping factor in Ta/Pt/Co multilayer films is attributable to an external mechanism. Given that the thickness of the Pt layer is greater than its spin diffusion length, the observed increase in the SOT efficiency is primarily attributed to the Pt layer. It can be reasonably assumed that an additional contribution is responsible for the observed decrease in magnetic damping [32, 33]. The sources of additional damping may include spin memory loss at the interface, magnetic proximity effect, spin-pumping

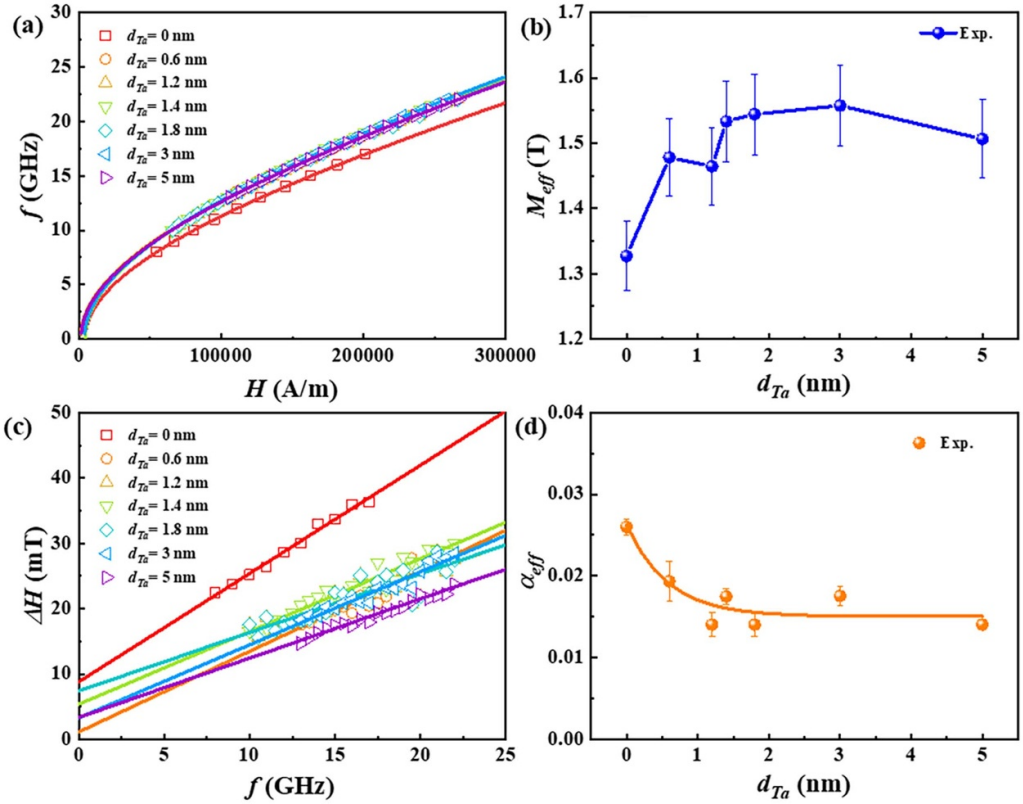

Figure 4. (a) The resonance field vs resonance frequency (a), the effective magnetization (b), the linewidth vs resonance frequency (c), and the effective damping factor (d) as a function of Ta capping layer thickness. The solid lines are fitting curves.

effect, and other factors. As the thickness of Ta increases, neither the thickness of Pt nor the Pt/Co interface changes. Consequently, the spin memory loss and magnetic proximity effects are primarily attributed to Pt/Co and can thus be excluded as a potential influencing factor. The spin-pumping effect is achieved by magnetization precession in the FM layer, which generates spin currents at the NM/FM interface. These spins transfer angular momentum to the neighboring NM layer, which functions as a spin sink by absorbing spin currents after crossing the spin diffusion length. This results in an enhancement of the Gilbert damping parameter. As the configuration of the Pt/Co interface remains unaltered, the spin–orbit coupling at this interface should also remain unaltered. Therefore, the observed weakening of the spin-pumping effect can be attributed to the reduction in the net spin current and the anti-damping raised from the REE [34].

Total magnetic damping from the spin-pumping effect includes contributions from the Pt and Ta layers, $\Delta\alpha_{\mathrm{sp\_tot}} = \alpha_{\mathrm{sp}}(\mathrm{Pt}) - \alpha_{\mathrm{sp}}(\mathrm{Ta})$. According to the spin pumping theory, the thickness dependence of the damping can be described by,

$$\Delta\alpha_{\mathrm{sp}} = \frac{g\mu_{\mathrm{B}}}{M_{\mathrm{s}}t} G^{\uparrow\downarrow}\left(1 - \mathrm{e}^{\frac{-2d}{\lambda_{\mathrm{sd}}}}\right) \tag{2}$$

where g is the spectroscopic splitting factor, μ_{B} is the Bohr magneton, $G^{\uparrow\downarrow}$ is the spin mixing conductance, and λ_{sd} is the spin diffusion length. The Pt and Ta layers are both spin sinks in the Ta/Pt/Co structure. Fitting the α_{eff} as a function of Ta capping layer thickness by equation (2), the obtained λ_{sd} and $G^{\uparrow\downarrow}$ are 1.16 nm and 15.7 nm^{-2}, respectively, which are close to the reported values of 1.5 nm and 15 nm^{-2} [35]. Liu *et al* also observed that the magnetic damping and the inhomogeneous linewidth broadening decrease with increasing Ta layer thickness in Ta/Cu/FeNi films [36].

Furthermore, using an in-plane damping-like SOT to reverse in-plane magnetization, the critical current density is given by [16], $J_{\mathrm{c0}} = M_{\mathrm{eff}}M_{\mathrm{S}}t_{\mathrm{FM}}\mathrm{e}\alpha/\hbar\theta_{\mathrm{SH}}^{\mathrm{eff}}$, which is proportional to $\alpha/\theta_{\mathrm{SH}}^{\mathrm{eff}}$. According to the results of figures 3(a) and 4(d), the J_{c0} of the Ta(1.2)/Pt(5)/Co(5) sample was only 54.0% than that of the Pt(5)/Co(5) sample. An improvement in the conversion efficiency from charge current to spin current in the device, as well as a lower critical current threshold and increased device lifetime and reliability, can be achieved by increasing the effective SOT efficiency and decreasing the effective magnetic damping constant [37].

4. Conclusions

In summary, our study demonstrates that by modulating the thickness of the capping layer in bilayers with opposite spin Hall angles, it is possible to diminish the magnetic damping factor while simultaneously achieving a substantial enhancement in SOT efficiency. This phenomenon might be attributed to the emergence of an additional SOT field generated by the interfacial REE. This stack design has significant potential to

advance our understanding and practical implementation of high-performance, low-power SOT-MRAM devices.

Data availability statement

All data that support the findings of this study are included within the article (and any supplementary files).

Supplementary data available at https://doi.org/10.1088/1361-648X/ae1d04/data1.

Acknowledgment

This work was supported by the Natural Science Foundation of Jiangsu Province (Grant No. BK20241447), the China Postdoctoral Science Foundation (Grant No. 2024M754138), and the Fundamental Research Funds for the Central Universities (Grant No. 30925010323). Z Xu was supported by Jiangsu Funding Program for Excellent Postdoctoral Talent (No. 2024ZB688). J Tang is supported by the Scientific Research Programs for High-level Talents Start-up Fund of Jinling Institute of Technology (jit-b-202361). We thank S C Hu for the discussion that led to this work. Finally, this paper is dedicated to my fifteen years at NJUST. As I prepare to leave, I am filled with memories of my younger self.

Author contributions

Zhan Xu 0000-0003-1224-9789
Conceptualization (equal), Data curation (equal), Investigation (equal), Methodology (equal), Writing – original draft (lead)

Shuo Wu 0000-0002-4112-737X
Data curation (equal), Methodology (equal)

Runtian Li 0009-0007-2181-7692
Investigation (equal), Methodology (equal)

Wenwen Liu 0009-0000-6962-3183
Formal analysis (equal), Validation (equal)

Er Liu 0000-0001-9534-7469
Data curation (equal), Visualization (equal)

Leixiang Bian 0000-0002-8248-586X
Writing – original draft (equal), Writing – review & editing (equal)

Feng Xu 0000-0001-5802-7925
Investigation (equal), Methodology (equal)

Jiaxuan Tang
Supervision (equal), Writing – review & editing (equal)

Wen Siang Lew 0000-0002-5161-741X
Supervision (equal), Writing – review & editing (equal)

References

[1] Ji G, Zhang Y, Chai Y and Nan T 2024 Recent progress on controlling spin-orbit torques by materials design *npj Spintronics* **2** 56
[2] Shao Q *et al* 2021 Roadmap of spin–orbit torques *IEEE Trans. Magn.* **57** 1–39
[3] Sinova J, Valenzuela S O, Wunderlich J, Back C H and Jungwirth T 2015 Spin Hall effects *Rev. Mod. Phys.* **87** 1213–60
[4] Song C, Zhang R, Liao L, Zhou Y, Zhou X, Chen R, You Y, Chen X and Pan F 2021 Spin-orbit torques: materials, mechanisms, performances, and potential applications *Prog. Mater. Sci.* **118** 100761
[5] Xu Z, Tang J, Hu S, Liu E, Xu F, Bian L and Lew W S 2024 Enhanced effective spin Hall efficiency contributed by the extrinsic spin Hall effect in $Pt_{1-x}Ta_x$/CoFeB structures *J. Appl. Phys.* **57** 145001
[6] Liu Q, Li J, Zhu L, Lin X, Xie X and Zhu L 2022 Strong spin-orbit torque induced by the intrinsic spin Hall effect in $Cr_{1-x}Pt_x$ *Phys. Rev. Appl.* **18** 054079
[7] Zhu L, Ralph D C and Buhrman R A 2021 Maximizing spin-orbit torque generated by the spin Hall effect of Pt *Appl. Phys. Rev.* **8** 031308
[8] Chen X *et al* 2021 Observation of the antiferromagnetic spin Hall effect *Nat. Mater.* **20** 800–4
[9] Li T, Jia W, Gao T, Haku S, Ye Z, Qiu M and An H 2022 Intrinsic spin Hall effect in oxidized platinum/magnetic oxide heterostructure *Appl. Phys. Lett.* **121** 132403
[10] Xu H *et al* 2020 High spin Hall conductivity in large-area type-II Dirac semimetal $PtTe_2$ *Adv. Mater.* **32** 2000513
[11] Wang X *et al* 2020 Spin transmission in IrMn through measurements of spin Hall magnetoresistance and spin-orbit torque *Phys. Rev. B* **101** 144412
[12] Zhu L, Ralph D C and Buhrman R A 2019 Enhancement of spin transparency by interfacial alloying *Phys. Rev. B* **99** 180404
[13] Han L *et al* 2022 Spin homojunction with high interfacial transparency for efficient spin-charge conversion *Sci. Adv.* **8** eabq2742
[14] Zhu L, Zhu L and Buhrman R A 2021 Fully spin-transparent magnetic interfaces enabled by the insertion of a thin paramagnetic NiO layer *Phys. Rev. Lett.* **126** 107204
[15] Gupta R *et al* 2025 Harnessing orbital Hall effect in spin-orbit torque MRAM *Nat. Commun.* **16** 130
[16] Huang L, He S, Yap Q J and Lim S T 2018 Engineering magnetic heterostructures to obtain large spin Hall efficiency for spin-orbit torque devices *Appl. Phys. Lett.* **113** 022402
[17] Ma Q, Li Y, Gopman D B, Kabanov Y P, Shull R D and Chien C L 2018 Switching a perpendicular ferromagnetic layer by competing spin currents *Phys. Rev. Lett.* **120** 117703
[18] Luan Z Z, Zhou L F, Wang P, Zhang S, Du J, Xiao J, Liu R H and Wu D 2019 Enhanced spin accumulation in metallic bilayers with opposite spin Hall angles *Phys. Rev. B* **99** 174406
[19] Hui Y, Jiang H, Xie F, Lin W, Dong C, Dong K, He Q and Miao X 2023 Maximizing spin Hall magnetoresistance in heavy metal/crystalline metallic ferromagnet multilayers with opposite spin Hall angles *Nanoscale* **15** 820–7
[20] Karube S, Tezuka N, Kohda M and Nitta J 2020 Anomalous spin-orbit field via the Rashba-Edelstein effect at the W/Pt interface *Phys. Rev. Appl.* **13** 024009
[21] Li T, Liu L, Li X, Zhao X, An H and Ando K 2023 Giant orbital-to-spin conversion for efficient current-induced magnetization switching of ferrimagnetic insulator *Nano Lett.* **23** 7174–9

[22] Xu Z, Wong G D H, Tang J, Liu E, Coester B, Xu F, Bian L and Lew W S 2023 The influence of Ti ultrathin insertion layer on the effective magnetic damping and effective spin Hall angle *Appl. Phys. Lett.* **122** 242405
[23] Kobayashi Y, Itoh T, Hisatomi R, Moriyama T, Shiota Y, Fan X and Ono T 2024 Spin-torque ferromagnetic resonance based on current-induced impedance *Appl. Phys. Lett.* **125** 022405
[24] Vasić B and Aškrabić S 2024 Thickness measurement of thin films using atomic force microscopy based scratching *Surf. Topogr.: Metrol. Prop.* **12** 025027
[25] Liu L, Moriyama T, Ralph D C and Buhrman R A 2011 Spin-torque ferromagnetic resonance induced by the spin Hall effect *Phys. Rev. Lett.* **106** 036601
[26] Bansal R, Chowdhury N and Muduli P K 2018 Proximity effect induced enhanced spin pumping in Py/Gd at room temperature *Appl. Phys. Lett.* **112** 262403
[27] Wong G D H, Ang C C I, Gan W, Law W C, Xu Z, Xu F, Seet C S and Lew W S 2021 Reversible strain-induced spin–orbit torque on flexible substrate *Appl. Phys. Lett.* **119** 042402
[28] Hsu J, Cheng C-W, Huang Y-H, Wu Y-H, Lin Y-L, Chang W-Y and Tseng Y-C 2024 Maximizing competing spin current of the W/Pt/ferromagnet devices with spin-torque ferromagnetic resonance analysis *2024 IEEE Int. Magnetic Conf.—Short Papers (INTERMAG Short Papers)* (IEEE) pp 1–2
[29] Kittel C 1948 On the theory of ferromagnetic resonance absorption *Phys. Rev.* **73** 155–61
[30] Liu E, Fache T, Cespedes-Berrocal D, Zhang Z, Petit-Watelot S, Mangin S, Xu F and Rojas-Sánchez J-C 2019 Strain-enhanced charge-to-spin conversion in Ta/Fe/Pt multilayers grown on flexible mica substrate *Phys. Rev. Appl.* **12** 044074
[31] He S *et al* 2017 Tunable magnetization relaxation of $Fe_2Cr_{1-x}Co_xSi$ half-metallic Heusler alloys by band structure engineering *Phys. Rev. Mater.* **1** 064401
[32] Caminale M, Ghosh A, Auffret S, Ebels U, Ollefs K, Wilhelm F, Rogalev A and Bailey W E 2016 Spin pumping damping and magnetic proximity effect in Pd and Pt spin-sink layers *Phys. Rev. B* **94** 014414
[33] Barati E and Cinal M 2017 Gilbert damping in binary magnetic multilayers *Phys. Rev. B* **95** 134440
[34] Behera N, Chaudhary S and Pandya D K 2016 Anomalous anti-damping in sputtered β-Ta/Py bilayer system *Sci. Rep.* **6** 19488
[35] Gómez J E, Zerai Tedlla B, Álvarez N R, Alejandro G, Goovaerts E and Butera A 2014 Spin transport parameters in $Ni_{80}Fe_{20}$/Ru and Ni_{80} Fe_{20}/Ta bilayers *Phys. Rev. B* **90** 184401
[36] Liu F, Zhou C, Tang R, Chai G and Jiang C 2021 Controllable charge-spin conversion by Rashba-Edelstein effect at Cu/Ta interface *J. Magn. Magn. Mater.* **540** 168462
[37] Lee D, Kim J, Park H, Lee K-J, Ju B-K, Koo H C, Min B-C and Lee O 2018 Spin-orbit torque and magnetic damping in tailored ferromagnetic bilayers *Phys. Rev. Appl.* **10** 024029